



Pyroxene standards for SIMS oxygen isotope analysis and their application to Merapi volcano, Sunda arc, Indonesia

Frances M. Deegan^{a,b,*}, Martin J. Whitehouse^b, Valentin R. Troll^a, David A. Budd^a, Chris Harris^c, Harri Geiger^a, Ulf Hålenius^b

^a Department of Earth Sciences, Centre for Experimental Mineralogy, Petrology, and Geochemistry (CEMPEG), Uppsala University, SE-75236 Uppsala, Sweden

^b Department of Geosciences, Swedish Museum of Natural History, SE-104 05, Stockholm, Sweden

^c Department of Geological Sciences, University of Cape Town, Rondebosch 7701, South Africa

ARTICLE INFO

Article history:

Received 30 May 2016

Received in revised form 30 September 2016

Accepted 8 October 2016

Available online 11 October 2016

Keywords:

Pyroxene crystals

SIMS standardisation

$\delta^{18}\text{O}$ analysis

Merapi volcano

Sub-Java primary $\delta^{18}\text{O}$

ABSTRACT

Measurement of oxygen isotope ratios in common silicate minerals such as olivine, pyroxene, feldspar, garnet, and quartz is increasingly performed by Secondary Ion Mass Spectrometry (SIMS). However, certain mineral groups exhibit solid solution series, and the large compositional spectrum of these mineral phases will result in matrix effects during SIMS analysis. These matrix effects must be corrected through repeated analysis of compositionally similar standards to ensure accurate results. In order to widen the current applicability of SIMS to solid solution mineral groups in common igneous rocks, we performed SIMS homogeneity tests on new augite (NRM-AG-1) and enstatite (NRM-EN-2) reference materials sourced from Stromboli, Italy and Webster, North Carolina, respectively. Aliquots of the standard minerals were analysed by laser fluorination (LF) to establish their $\delta^{18}\text{O}$ values. Repeated SIMS measurements were then performed on randomly oriented fragments of the same pyroxene crystals, which yielded a range in $\delta^{18}\text{O}$ less than ± 0.42 and $\pm 0.58\%$ (2σ) for NRM-AG-1 and NRM-EN-2, respectively. Homogeneity tests verified that NRM-AG-1 and NRM-EN-2 do not show any crystallographic orientation bias and that they are sufficiently homogeneous on the 20 μm scale to be used as routine mineral standards for SIMS $\delta^{18}\text{O}$ analysis. We subsequently tested our new standard materials on recently erupted pyroxene crystals from Merapi volcano, Indonesia. The $\delta^{18}\text{O}$ values for Merapi pyroxene obtained by SIMS ($n = 204$) agree within error with the LF-derived $\delta^{18}\text{O}$ values for Merapi pyroxene but differ from bulk mineral and whole-rock data obtained by conventional fluorination. The bulk samples are offset to higher $\delta^{18}\text{O}$ values as a result of incorporation of mineral and glass inclusions that in part reflects crustal contamination processes. The Merapi pyroxene SIMS data, in turn, display a frequency peak at 5.8‰, which allows us to estimate the $\delta^{18}\text{O}$ value of the primary mafic magma at Merapi to $\sim 6.1\%$ when assuming closed system differentiation.

© 2016 Elsevier B.V. All rights reserved.

1. Introduction

Developments in Secondary Ionisation Mass Spectrometry (SIMS) have allowed measurement of oxygen isotope ratios of sample pit sizes $< 20 \mu\text{m}$ diameter with precision down to $\pm 0.3\%$ (2σ) on silicate, oxide, and carbonate geo-materials (e.g. minerals, glass, experimental products; cf. Page et al., 2007; Valley and Kita, 2009; Whitehouse and Nemchin, 2009; Valley et al., 2015). Oxygen isotope SIMS studies have thus far been carried out on a wide range of terrestrial and extra-terrestrial materials, including igneous and metamorphic zircon (e.g. Bindeman

and Valley, 2000; Nemchin et al., 2006a), garnet (e.g. Page et al., 2010; Ferry et al., 2014), calcite, dolomite-ankerite, kyanite and wollastonite (Ferry et al., 2014; Śliwiński et al., 2016), olivine and feldspar (e.g. Gurenko and Chaussidon, 2002; Mora et al., 2009; Eiler et al., 2011; Winpenny and Maclennan, 2014), quartz (e.g. Valley and Graham, 1996; Hyodo et al., 2014), volcanic glass and melt inclusions (e.g. Gurenko and Chaussidon, 2002; Hartley et al., 2012), lunar zircon (Nemchin et al., 2006b; Whitehouse and Nemchin, 2009), and silicic meteoritic clasts and martian carbonates (Kita et al., 2004; Nemchin et al., 2014). However, in depth studies of oxygen isotope variability in magmatic pyroxene by SIMS are thus far lacking because of the limited availability of suitable standard materials. Important issues to overcome with standardisation are instrumental mass fractionation (IMF) and matrix effects, especially for a given solid-solution mineral, where a degree of bias may be caused by the major element composition and the crystallographic orientation of the sample. These issues can be overcome by employing repeated analysis of composition-matched

* Corresponding author at: Department of Earth Sciences, Centre for Experimental Mineralogy, Petrology, and Geochemistry (CEMPEG), Uppsala University, 75236 Uppsala, Sweden.

E-mail addresses: Frances.Deegan@geo.uu.se (F.M. Deegan), Martin.Whitehouse@nrm.se (M.J. Whitehouse), Valentin.Troll@geo.uu.se (V.R. Troll), David.Budd@geo.uu.se (D.A. Budd), Chris.Harris@uct.ac.za (C. Harris), Harri.Geiger@geo.uu.se (H. Geiger), Ulf.Halenius@nrm.se (U. Hålenius).

standards during the analytical session (e.g. Eiler et al., 1997; Valley and Kita, 2009; Page et al., 2010) or by linearly interpolating bias based on systematic changes in crystal chemistry (cf. Riciputi et al., 1998; Kita et al., 2004). However, correcting for matrix effects is particularly challenging for mineral groups that show a range of solid solution compositions, such as pyroxene, feldspar, or garnet. In these cases, a suite of standards are required to either match the composition of the analyte or model mass bias as a function of major element chemical variation (e.g. Riciputi et al., 1998; Valley and Kita, 2009; Page et al., 2010).

While mineral and glass standards for oxygen isotope analysis are well characterised for some compositions, e.g., zircon and basaltic glass (Wiedenbeck et al., 2004; Jochum et al., 2006; Sláma et al., 2008; Hartley et al., 2012), relatively few reliable mineral standards are available for common pyroxene. Perhaps the most widely available pyroxene standard is JV1 diopside (Eiler et al., 1997), but JV1 alone is not always adequate due to the fact that several distinct pyroxene compositions may be present in a single magmatic rock. For instance, arc basaltic-andesites often contain mixed populations of calcic clinopyroxene and orthopyroxene, as is the case for several volcanoes along the Sunda arc subduction zone in Indonesia (e.g. Gede volcano, Handley et al., 2010; Krakatau volcano, Dahren et al., 2012; Merapi volcano, Borisova et al., 2013; Troll et al., 2013; Kelut volcano, Jeffery et al., 2013). In previous studies pyroxene has been shown to exhibit large ranges in IMF of ca. 5‰ from enstatite to wollastonite (Valley and Kita, 2009; Eiler et al., 2011) and so it is crucial that pyroxene standards covering a more complete range of natural endmember compositions are made available to better calibrate for the effect of matrix effects during SIMS analysis. When investigating the oxygen isotope composition of igneous pyroxene, the approach in this paper is to utilise multiple mineral standards in order to match the composition to the unknown as closely as possible and thereby minimise attendant corrections and error propagations (cf. Eiler et al., 1997; Valley and Kita, 2009).

The aims of this study are therefore to firstly characterise new mineral standards for calcic clinopyroxene (augite; NRM-AG-1) and orthopyroxene (enstatite; NRM-EN-2) for use in SIMS studies to complement the currently available JV1 diopside standard (cf. Eiler et al., 1997) and various in-house pyroxene standards hosted by a number of individual SIMS laboratories worldwide (e.g. Wisc SIMS). Secondly, an example of oxygen isotope analysis of magmatic pyroxene is presented for the 2006 basaltic-andesite eruption at Merapi volcano, Indonesia, using the NRM-AG-1 and JV1 diopside standards. We then compare our new Merapi SIMS data to data obtained from the same eruption products by laser fluorination of pyroxene and conventional fluorination of pyroxene mineral separates and whole-rock powders (cf. Troll et al., 2013) in order to assess the robustness and benefits of the SIMS approach.

2. Sample selection and preparation

2.1. Homogeneity test mounts

Pyroxene crystals were selected from the mineral collection at the Swedish Museum of Natural History (NRM), Stockholm, Sweden, for use as standards in this study. Candidate crystals were chosen for their differing compositions (augite versus enstatite), and were of relatively large size (several cm) to enable their eventual distribution as standard material. An augite specimen from Stromboli, Italy was collected by Mr. Karl Johansson from Hedemora, Sweden and donated to the NRM in 1927 (catalogue number NRM#19270125) and is called NRM-AG-1 in this study. This specimen contains a large number of up to several centimetre sized augite crystals and a minor quantity of volcanic ash. A monomineralic enstatite specimen consisting of an aggregate of centimetre sized crystals from Webster, North Carolina was donated to the NRM by the Smithsonian National Museum of Natural History, USA. The enstatite specimen has the catalogue number NRM#18890193

(original US National Museum catalogue number is #47530) and is referred to as NRM-EN-2 in this study.

The pyroxene specimens for standardisation were crushed by hand into mm-sized fragments and several aliquots were prepared by hand-picking under a binocular microscope. One split of the crystal fragments was analysed by laser fluorination (LF, see below) and another split was carefully mounted in epoxy resin under an optical microscope, avoiding a preferred orientation of long-axes and cleavage planes, which could introduce a systematic bias in the SIMS homogeneity tests. The mounts were then cast in epoxy resin and polished using an automated polishing machine and employing progressively fining diamond suspensions (down to 1 µm for the final polishing step). Great care was taken to ensure that crystals were placed within a distance of >5 mm from the edge of the mount, and that the mount was polished flat with minimal relief in order to avoid analytical artifacts associated with sample geometry and topography (Fig. 1; Kita et al., 2009; Whitehouse and Nemchin, 2009). Finally, the sample mounts were coated with carbon for Electron Probe Micro Analysis (EPMA), after which the carbon coat was removed from the sample mount by polishing the surface with a 1 µm diamond solution. The sample mount was then cleaned with pure ethanol and coated with a 20 nm gold layer prior to SIMS analysis.

2.2. Merapi pyroxene mounts

Merapi volcano is an active stratovolcano located on Java Island above the Sunda arc subduction zone. Most of its recent eruption products consist of block-and-ash type flows of basaltic-andesite composition within which feldspar and clinopyroxene are the major phenocrysts phases (e.g. Gertisser and Keller, 2003; Chadwick et al., 2007, 2013; Costa et al., 2013; Troll et al., 2013; van der Zwan et al., 2013; Preece et al., 2014). The basaltic-andesite samples chosen for this study were erupted in 2006 and previously analysed for their oxygen isotope ratios by conventional fluorination of whole-rock and bulk pyroxene and bulk feldspar mineral separates (samples M-BA06-KA1 and M-BA-06-KA4 in Troll et al., 2013). In addition, a number of pyroxene crystals from other samples of Merapi's recent eruptive products were analysed by laser fluorination by Troll et al. (2013), providing a useful comparative framework for our investigation. Grain mounts containing hand-picked pyroxene crystals extracted from the 2006 rock samples

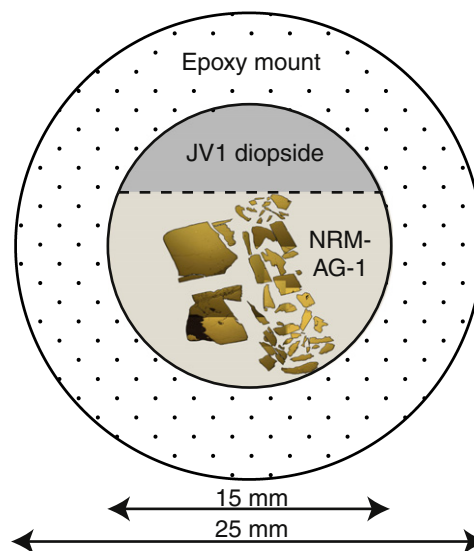


Fig. 1. Sketch of the mount prepared for the NRM-AG-1 homogeneity test by SIMS, containing randomly oriented pyroxene crystal fragments and the JV1 diopside standard. The test mount for NRM-EN-2 was prepared in the same manner. Care was taken to ensure optimal sample geometry and topography (see text for details).

were prepared for EPMA and SIMS analysis in a similar fashion to the standard materials described above, thus providing a well-characterised natural test study.

3. Analytical methods

3.1. EPMA and Mössbauer analysis of pyroxene

Mineral chemical data were acquired using the field-emission source JEOL JXA-8530F Hyperprobe (FEG-EPMA) at the Centre for Experimental Mineralogy, Petrology and Geochemistry (CEMPEG), Uppsala University, Sweden. The run conditions were 15 kV accelerating voltage and 10 nA probe current with 10 s on peak and 5 s on lower and upper background, with a beam diameter for 2 μm for pyroxene analysis. The following standards were used for calibration: wollastonite for Ca and Si, pyrophanite (MnTiO_3) for Mn and Ti, magnesium oxide for Mg, orthoclase for K, albite for Na, aluminium oxide for Al, fayalite for Fe, nickel oxide for Ni, and chromium oxide for Cr. Analytical precision was measured on Smithsonian Institute mineral standards, including USNM 111312 (olivine), USNM 122142 (Cr-augite), USNM 137041 (anorthite), USNM 115900 (Ca-plagioclase), and USNM 133868 (anorthoclase). Uncertainties on the standards are as follows: SiO_2 , Al_2O_3 , MgO and $\text{CaO} \leq 1.5\%$ s.d., $\text{FeO} \leq 2.2\%$ s.d., Na_2O in plagioclase and clinopyroxene $\leq 4.5\%$ s.d., and minor elements $\leq 10\%$ s.d. Further details can be found in [Barker et al. \(2015\)](#).

A room-temperature ^{57}Fe Mössbauer spectrum was recorded on powdered clinopyroxene NRM-AG-1 using a WISSEL MA260S Mössbauer instrument operating in constant acceleration mode. The sample absorber consisting of ca. 5 mg mineral powder mixed with a thermoplastic polymer was placed close to a ^{57}Co source in a rhodium matrix with a nominal activity of 50 mCi. The spectrum was collected over the velocity range -4.2 to $+4.2$ $\text{mm}\cdot\text{s}^{-1}$ and was calibrated against α -Fe foil before folding and spectral fitting with the software MossA ([Prescher et al., 2012](#)).

3.2. Oxygen isotope analysis by laser fluorination (LF)

Mineral grains were prepared by hand-picking clean, inclusion-poor crystals under a binocular microscope. Laser fluorination of NRM-AG-1 ($n = 2$), NRM-EN-2 ($n = 2$), Merapi pyroxene extracted from basaltic-andesite lava ($n = 2$), and Merapi pyroxene extracted from a coarse grained cumulate ($n = 2$) were then carried out in the Department of Geological Sciences, University of Cape Town (UCT), South Africa, using pyroxene fragments weighing ca. 2 mg for each independent run. The oxygen isotope results are reported in standard δ -notation relative to SMOW (Standard Mean Ocean Water), where $\delta = [({}^{18}\text{O}/{}^{16}\text{O})_{\text{sample}} / ({}^{18}\text{O}/{}^{16}\text{O})_{\text{SMOW}} - 1] * 1000$. Full analytical details of the laser fluorination method employed at UCT are given in [Harris and Vogeli \(2010\)](#). Measured values of the UCT internal standard MON GT (Monastery garnet, $\delta^{18}\text{O} = 5.38\%$, [Harris and Vogeli, 2010](#)) were used to normalise the raw data and correct for drift in the reference gas. The $\delta^{18}\text{O}$ value of MON GT was established by cross-calibration with the UWG-2 garnet standard of [Valley et al. \(1995\)](#) and San Carlos olivine. The average difference in $\delta^{18}\text{O}$ values of duplicates of MON GT analysed during this study was 0.14‰, which corresponds to a 2 σ value of 0.19‰. Oxygen isotope analysis of Merapi pyroxene mineral separates and basaltic-andesite whole-rock powders were also carried out at UCT, South Africa using conventional fluorination as described in [Troll et al. \(2013\)](#). The published Merapi data are thus fully comparable to our new SIMS data presented in [Section 4.2](#).

3.3. SIMS analytical technique

Following preparation (see [Section 2.1](#)), the mounted pyroxene crystals were analysed for their oxygen isotope ratios by SIMS at the Nordsim ion microprobe facility, Swedish Museum of Natural History,

Stockholm, using a CAMECA IMS 1280 multi-collector equipped instrument. The standard crystals were analysed during the course of two separate analytical sessions in 2014. One session was dedicated to testing the homogeneity of the augite and the other to test the enstatite standard, in each case in random orientations, i.e. independently of crystallographic axes. Another potential enstatite standard from the mineral collection at NRM (from Stakholmen, Sweden, with catalogue number #19930489) was analysed during a third analytical session, but was subsequently rejected from this study due to an unacceptable degree of isotopic heterogeneity and is not discussed further. The Merapi pyroxenes were analysed in 2014 during a fourth analytical session after establishing the suitability of NRM-AG-1 and NRM-EN-2.

The SIMS instrumentation and methods employed here are based on [Nemchin et al. \(2006a\)](#) and [Whitehouse and Nemchin \(2009\)](#), incorporating within-run beam centering in the field aperture using the transfer deflectors. A 20 keV Cs^+ primary beam of ca. 2.5 nA was used in critically-focussed mode together with a 5 μm raster to sputter a ca. 10 μm sample area. A normal incidence low energy electron gun provided charge compensation. The runs comprised a 90 s pre-sputter period with a raster of 20 μm , and field aperture centring using ^{16}O signal followed by 64 s (16 cycles of 4 s integrations) of data acquisition using two Faraday detectors in the multicollector system that operated at a common mass resolution of ca. 2500. The secondary magnet field was regulated at high precision using a Metrolab NMR teslameter.

For the pyroxene homogeneity tests, one of the crystal fragments was designated as an internal reference (or running standard), which was intermittently analysed throughout the analytical sessions and bracketed the unknown sample analyses to monitor instrument drift. Specifically, two running standards were analysed before and after every six unknown analyses, which included one analysis of JV1 and five analyses of the pyroxene unknowns. To monitor external reproducibility in the Merapi analytical sessions, a similar sample-bracketing procedure was used, except that every block of four sample analyses was bracketed before and after by two standard analyses. In all analytical sessions, the running standard was assigned the $\delta^{18}\text{O}$ value determined by LF and the ratios of the remaining values obtained were normalised to the LF values as follows.

Standard analyses were separated from analyses of unknown samples and their raw $^{18}\text{O}/^{16}\text{O}$ ratios were plotted in a time sequence. Any analytical drift was then modelled, typically as a minor linear function. Assuming a homogeneous standard, this step yielded an average $^{18}\text{O}/^{16}\text{O}$ value together with a standard deviation representing external precision (σ_{ext}). All raw $^{18}\text{O}/^{16}\text{O}$ ratios were subsequently drift corrected in a similar fashion. The corrected $^{18}\text{O}/^{16}\text{O}$ ratios were then converted to $\delta^{18}\text{O}$ values using Eq. (1) after [Hoefs \(1973\)](#),

$$\delta \text{ in } \text{‰} = \frac{R(\text{sample}) - R(\text{standard})}{R(\text{standard})} 1000, \quad (1)$$

where R is the measured $^{18}\text{O}/^{16}\text{O}$ ratio. The $\delta^{18}\text{O}$ values relative to the SMOW scale were then calculated using the $\delta^{18}\text{O}$ values resulting from Eq. (1) and the $\delta^{18}\text{O}$ values of the standard determined by laser fluorination, as follows,

$$\delta_{X-A} = \left[\left(\frac{\delta_{B-A}}{1000} + 1 \right) \left(\frac{\delta_{X-B}}{1000} + 1 \right) - 1 \right] 1000, \quad (2)$$

where X is the sample and A and B are the different standards (after [Hoefs, 1973](#)). Finally, the overall uncertainty (σ_{tot}) of each analysis was calculated by a quadrature addition of the within run standard error of the mean on the $^{18}\text{O}/^{16}\text{O}$ ratio returned by the CAMECA instrument running software (σ_{int} based on 16 cycles) and the external standard deviation (σ_{ext}) as described above, i.e.,

$$\sigma_{\text{tot}} = (\sigma_{\text{int}}^2 + \sigma_{\text{ext}}^2)^{0.5}. \quad (3)$$

In order to determine IMF (Δ , given in ‰), which is the difference between the true isotope ratio of a reference material and the measured ratio, the true $^{18}\text{O}/^{16}\text{O}$ ratio of the reference material is determined from its $\delta^{18}\text{O}$ (SMOW) value using the accepted $^{18}\text{O}/^{16}\text{O}$ ratio of SMOW of 0.0020052 (Baertschi, 1976). The IMF depends on instrument tuning parameters and is constant for a given session but may vary between sessions. Note that the IMF for a measured sample and a standard will be the same if both are of exactly the same composition. For the Merapi analytical sessions, IMF corrections reached a maximum of 0.15‰, but were frequently much lower (see Supplementary Table 4). If the sample composition differs significantly from that of the standard, however, there will be a bias in the apparent IMF related to the way different matrices sputter. Correcting for this effect is complex in solid solution mineral groups such as pyroxene and IMF-bias curves are normally employed to calibrate the sample to the standard (cf. Tenner et al., 2013). In this study, we have aimed to use standards that are closely matrix-matched to the unknown samples, thus avoiding complex matrix corrections that would introduce additional error in the analysis.

In total, fourteen separate grains (79 SIMS spots) of NRM-AG-1 and eight separate grains (76 SIMS spots) of NRM-EN-2 were analysed in the homogeneity tests. The JV1 diopside standard (Eiler et al., 1997) was also analysed throughout each session, as an external monitor of potential drift in IMF during the session ($n = 11$ analyses per homogeneity test session). The SIMS homogeneity tests yielded a range in $\delta^{18}\text{O}$ less than ± 0.42 and 0.58% (2σ) for NRM-AG-1 and NRM-EN-2, respectively and average ^{16}O intensities were 2.14×10^9 counts per second (cps) and 1.65×10^9 cps for each test session, respectively. Throughout the Merapi pyroxene analytical session, external reproducibility (2σ mean) ranged from 0.30 to 0.42‰. Internal precision or spot to spot reproducibility (2σ) ranged from $\pm 0.32\%$ to 0.46‰ (RSD; $n = 51$) and $\pm 0.42\%$ to 0.54‰ (RSD; $n = 57$) on NRM-AG-1 and JV1, respectively. The average ^{16}O intensity in the Merapi session was 2.5×10^9 cps. We also note that all sample mounts were analysed by Scanning Electron Microscopy (SEM) imaging before analysis to create sample maps to aid placement of analysis pits on clean areas. Finally, all mounts were analysed by optical microscopy after analysis to verify that analysis spots were not placed on fractures or foreign phases, however, it is possible that small inclusions of foreign material may have occasionally occurred in the sample volume (see also Sections 4.2 and 5.2.1 for discussion of five outlier values).

4. Results

4.1. NRM-AG-1 and NRM-EN-2

The major element compositions of standards NRM-AG-1, NRM-EN-2, and JV1 are presented in Supplementary Table 1 and illustrated in Fig. 2. The SIMS instrument set-up (stage position and field aperture), drift-corrected $^{18}\text{O}/^{16}\text{O}$ ratios, and $\delta^{18}\text{O}$ values obtained during the standard homogeneity tests are given in Supplementary Table 2. The corrected results of the homogeneity tests are shown in Fig. 3, where it can be seen that repeated SIMS measurements on randomly oriented fragments of the pyroxene crystals yielded a range in $\delta^{18}\text{O}$ less than ± 0.42 and 0.58% (2σ) for NRM-AG-1 and NRM-EN-2, respectively. Duplicate analysis of the standard minerals by LF gave $\delta^{18}\text{O}$ values of 5.4 and 5.5‰ (average of 5.5‰) for NRM-AG-1 and 5.5 and 5.7‰ (average of 5.6‰) for NRM-EN-2.

4.2. Merapi pyroxene results

The major element compositions of Merapi 2006 pyroxene are presented in Supplementary Table 3 and illustrated in Fig. 4. We analysed a total of 32 pyroxene crystals ($n = 209$ individual spot analyses) for their oxygen isotope ratios (see Supplementary Table 4). As Merapi pyroxene are generally inclusion-rich, particular care was taken to avoid

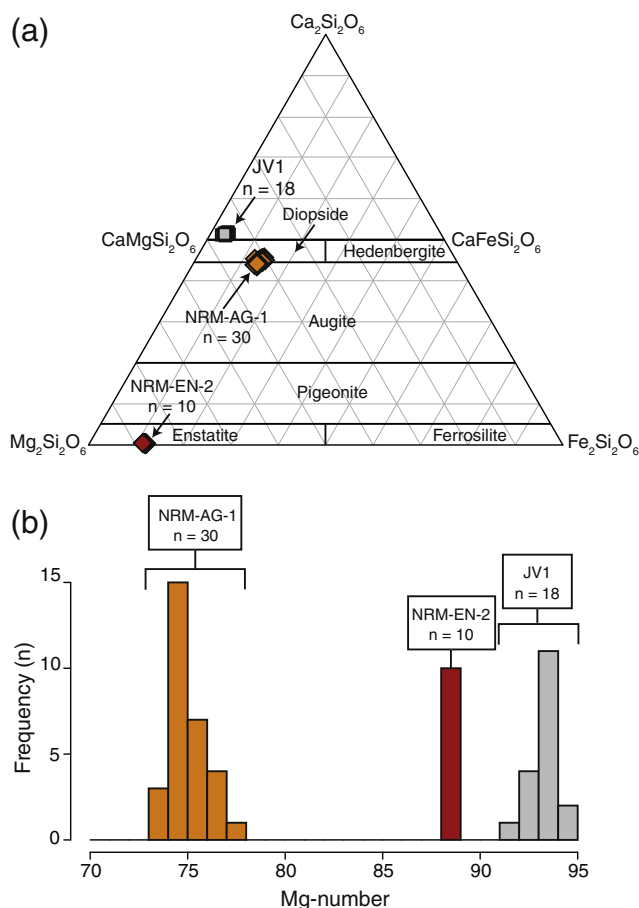


Fig. 2. (a) Composition of NRM-AG-1, NRM-EN-2, and JV1 determined by EPMA. Multiple analyses were performed on individual crystal fragments. (b) Frequency distribution plot showing the limited range in Mg-number (defined as $100\text{MgO} / (\text{MgO} + \text{FeO})$) of the individual standards and the relatively large differences in Mg-number between the different standards.

placing analysis spots on mineral or melt inclusions, on fractures, and near the edge of crystals (Fig. 4b). Merapi pyroxene exhibit an overall range in $\delta^{18}\text{O}$ values from 4.3 to 8.1‰ (average $\delta^{18}\text{O} = 5.8 \pm 1.2\%$, 2SD), respectively (see also Section 5.2.1 for discussion of data reduction). Note that four spot analyses from two separate crystals with $\delta^{18}\text{O}$ values $< 3\%$ and one analysis with a $\delta^{18}\text{O}$ value of 4‰ were omitted as outliers. The cause of these outliers is unknown, but it is possible that these analyses accidentally sampled foreign material in the pyroxene. The remaining SIMS data ($n = 204$) overlap with the $\delta^{18}\text{O}$ values of Merapi 2006 pyroxene crystals obtained by LF, which range from 5.1 to 5.8‰ ($n = 4$, average $\delta^{18}\text{O} = 5.4\%$, Troll et al., 2013, Fig. 5). In turn, Merapi bulk pyroxene separates (representing 10's to 100's of crystals) have $\delta^{18}\text{O}$ values ranging from 5.9 to 7.2‰ ($n = 7$, average $\delta^{18}\text{O} = 6.7\%$, Troll et al., 2013), and Merapi whole-rocks have $\delta^{18}\text{O}$ values ranging from 5.6 to 8.3‰ ($n = 32$, average $\delta^{18}\text{O} = 6.9\%$, Troll et al., 2013, see Fig. 5).

We also carried out clinopyroxene composition barometry using Eq. (32b) in Putirka (2008) on all pyroxenes analysed for oxygen isotopes by SIMS in this study. The Putirka (2008) formulation is a recalibration of the Nimis (1995) model, which removes the systematic error by incorporating a H_2O content. We assumed a H_2O content of 6 wt.% based on clinopyroxene hygrometry on sample M-BA06-KA4 by Weis et al. (2016). The thermobarometry results show a crystallisation pressure range from 253 to 601 MPa, with a frequency peak at 470 MPa (standard error of estimate = ± 260 MPa; see Section 5.2).

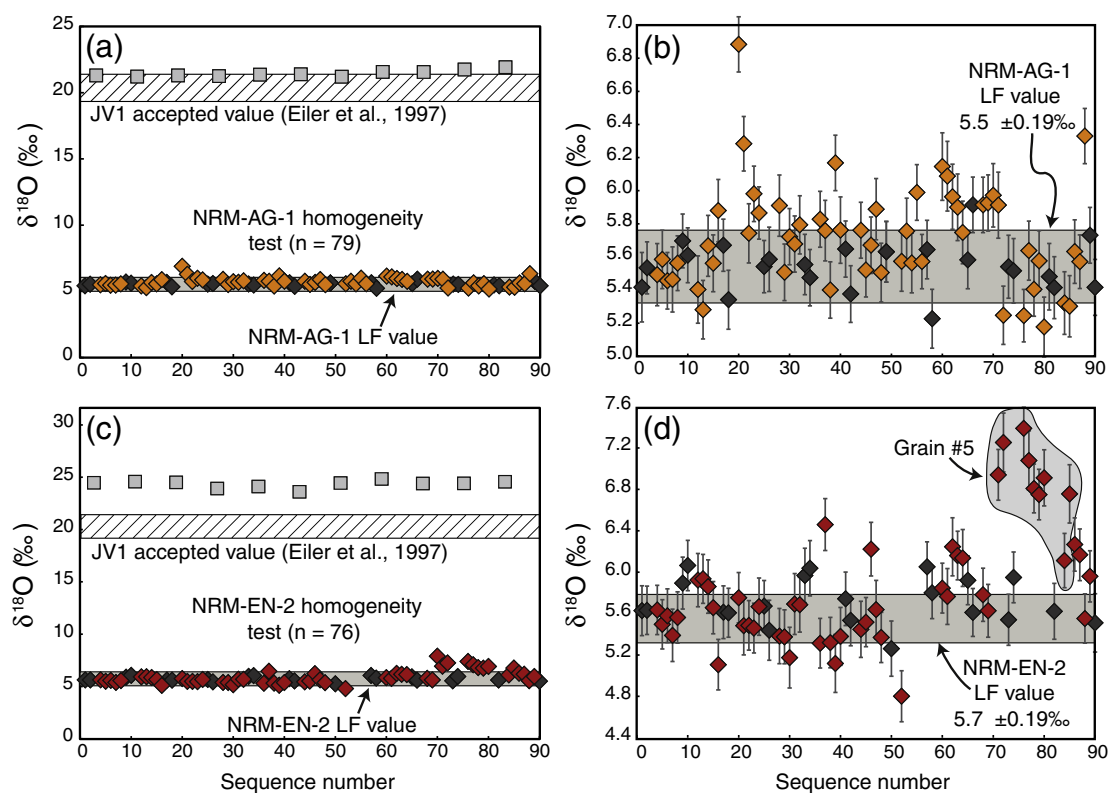


Fig. 3. IMF-corrected results of SIMS homogeneity tests on randomly oriented fragments of NRM-AG-1 (a, b) and NRM-EN-2 (c, d). Analyses of the designated reference grain for each of NRM-AG-1 and NRM-EN-2 are presented with black symbol colour. Note that analysis of JV1 diopside (grey squares) was calibrated to both NRM-AG-1 and NRM-EN-2 and yielded inaccurate results due to matrix effects when calibrated against the enstatite. Fourteen individual grains of NRM-AG-1 and eight grains of NRM-EN-2 were employed in the homogeneity tests. In the case of NRM-EN-2, one grain yielded abnormally high $\delta^{18}\text{O}$ values (grain 5, highlighted). Error on data in panels (a, c) is smaller than symbol size; error bars in panels (b, d) are 1 σ .

5. Discussion

5.1. Assessment of standard material

Fragments of the minerals NRM-AG-1, NRM-EN-2, and JV1 were analysed in randomly selected spots by EPMA. The data show low within-crystal major element variability (Supplementary Table 1), as demonstrated by relatively restricted ranges in Mg-numbers (Fig. 2). NRM-AG-1 has greater Mg-number variability than NRM-EN-2 and JV1, but the majority of values cluster around 74 to 75, 88, and 93 to 94 for the three minerals, respectively. None of the minerals examined showed evidence of internal zoning in Back Scattered Electron (BSE) imaging and only NRM-AG-1 contains small (mostly < 10 μm across), volumetrically minor melt inclusions in some of the mounted fragments. The inclusions in NRM-AG-1 are thought to be insufficient to influence the $\delta^{18}\text{O}$ value of the mineral obtained by LF outside the limits of the analytical uncertainty associated with the LF method.

To test NRM-AG-1 and NRM-EN-2 for isotopic homogeneity we performed repeated SIMS analysis on fragments of pristine crystalline material, taking care to avoid cracks and inclusions. We did not perform this step on the JV1 standard, as it is already an accepted reference material. We specifically analysed multiple fragments of each of NRM-AG-1 and NRM-EN-2 along no preferred crystallographic orientation because some mineral groups such as magnetite are known to demonstrate strong crystal orientation effects (cf. Huberty et al., 2010). However, bias due to crystal orientation is usually thought to be minimal for most silicate minerals (Valley and Kita, 2009), and our data confirm that orientation effects are indeed minimal for the investigated pyroxene crystals. Moreover, the SIMS homogeneity tests demonstrate that NRM-AG-1 and NRM-EN-2 display low variance in their $\delta^{18}\text{O}$ values (0.08‰ for NRM-AG-1 and 0.32‰ for NRM-EN-2) and are thus

sufficiently homogeneous with respect to their $\delta^{18}\text{O}$ values at the 20 μm sampling scale to be used as mineral standards for SIMS (Fig. 3). We note that one out of eight grains of NRM-EN-2 yielded $\delta^{18}\text{O}$ values that deviated from all other analyses in that session (grain 5 highlighted in Fig. 3d). The source of this deviation is unknown and may represent a minor degree of real heterogeneity in the standard material (1 grain of 8). Discarding this particular grain, the variance in $\delta^{18}\text{O}$ values becomes 0.09‰, and thus similar to that for NRM-AG-1.

Because our mineral samples show limited major element variability we could not test for variations in instrumental mass fractionation (IMF) with composition. We nonetheless suggest that pyroxene composition is determined precisely to ensure accurate $\delta^{18}\text{O}$ determination by SIMS, as utilising composition-matched standards is the safest approach to ensure robust data (e.g. Eiler et al., 1997). This caveat is highlighted by our analyses of the JV1 diopside standard during the homogeneity tests. As seen in Fig. 3, the accepted value of 20.3‰ for JV1 was not reproduced accurately in our test sessions due to the differing matrix effects between diopside and augite or enstatite (see Section 5.2.1).

5.2. Application: $\delta^{18}\text{O}$ variations in pyroxene from the Merapi 2006 eruption

5.2.1. Data reduction and assessment

Merapi pyroxene crystals were mounted with the NRM-AG-1 (augite) and JV1 (diopside) standards and 32 individual crystals were analysed for their $\delta^{18}\text{O}$ values ($n = 209$ spot analyses, of which 5 spots were rejected as outliers as they may have accidentally sampled non-pyroxene material. See also Section 4.2 and rejected analyses in italics in Supplementary Table 4). To compare the outcome of using our new standard versus the established JV1 standard, analyses of augitic Merapi pyroxene were bracketed by repeated analyses of NRM-AG-1, whereas slightly more

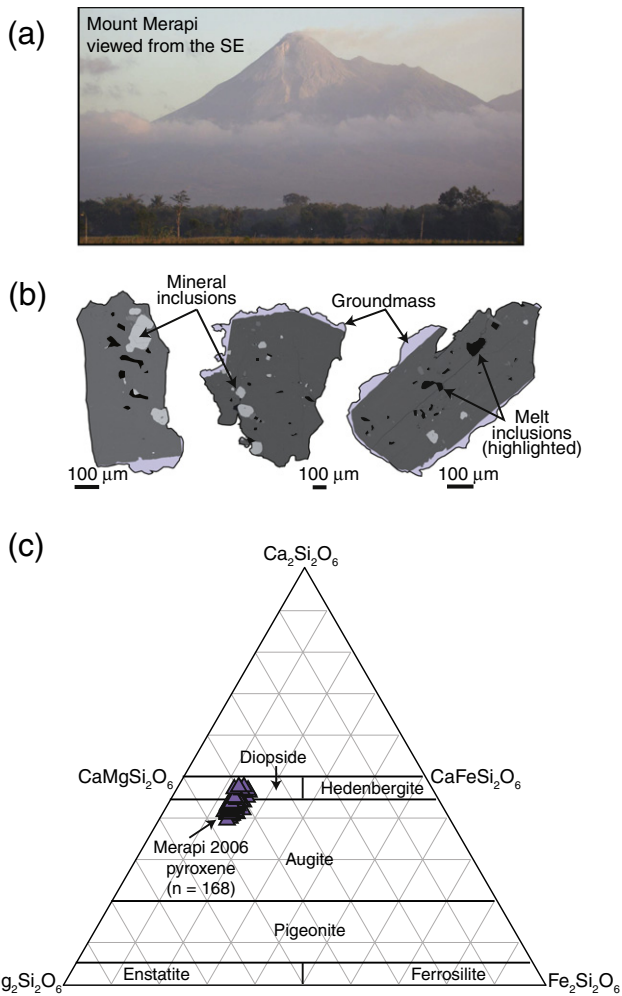


Fig. 4. (a) Photo of Merapi volcano, Central Java, Indonesia after Troll et al. (2015). Note the visible open crater. (b) Scanning Electron Microscopy (SEM) images of representative 2006 Merapi pyroxene with clearly visible mineral (bright grey) and melt inclusions (highlighted in black) and adhered groundmass (highlighted in pale purple), which could distort the $\delta^{18}\text{O}$ values obtained using bulk crystal analysis. Using the SIMS approach, we ensured “pure” pyroxene $\delta^{18}\text{O}$ analyses, by avoiding inclusions, fractures, and groundmass. (c) Composition of Merapi pyroxene from the 2006 eruption determined by EPMA.

calcic pyroxene crystals were bracketed by JV1 (cf. Figs. 2 and 4). Merapi pyroxene values corrected to NRM-AG-1 range in $\delta^{18}\text{O}$ from 4.6 to 7.4‰ (average of 5.77‰ and 2SD of 1.03‰) and overlap the previously obtained $\delta^{18}\text{O}$ values of Merapi pyroxene using the LF method (Fig. 5). This result serves as an external validation of our new standard and verifies the accuracy of the SIMS data. When corrected to the accepted JV1 value of 20.3‰ (Eiler et al., 1997), the more calcic Merapi pyroxene yielded $\delta^{18}\text{O}$ values that range from 3.2 to 7.0‰ with an average of 5.0‰. These values are skewed towards relatively low values compared to Merapi augite analysed by SIMS and Merapi pyroxene analysed by LF. The apparent bias towards lower $\delta^{18}\text{O}$ values in the calcic pyroxene data set is surprising because under equilibrium conditions oxygen isotopes are not known to fractionate between e.g., augite and diopside crystals (which are structurally similar) in the same rock sample (e.g. Chiba et al., 1989). To understand this discrepancy between data sets, we note that the accepted value of JV1 was not accurately reproduced in the NRM-AG-1 homogeneity test session (Fig. 3a), most likely because of the matrix effects involved in using NRM-AG-1 to correct the JV1 values, as these two minerals do not have the same composition and would sputter differently during SIMS analysis (see Supplementary Table 2 and Figs. 2 and 4). In the NRM-AG-1 homogeneity test, we obtained systematically higher JV1 values than those reported in Eiler et al. (1997), with an average of 21.4‰ (Fig. 3a).

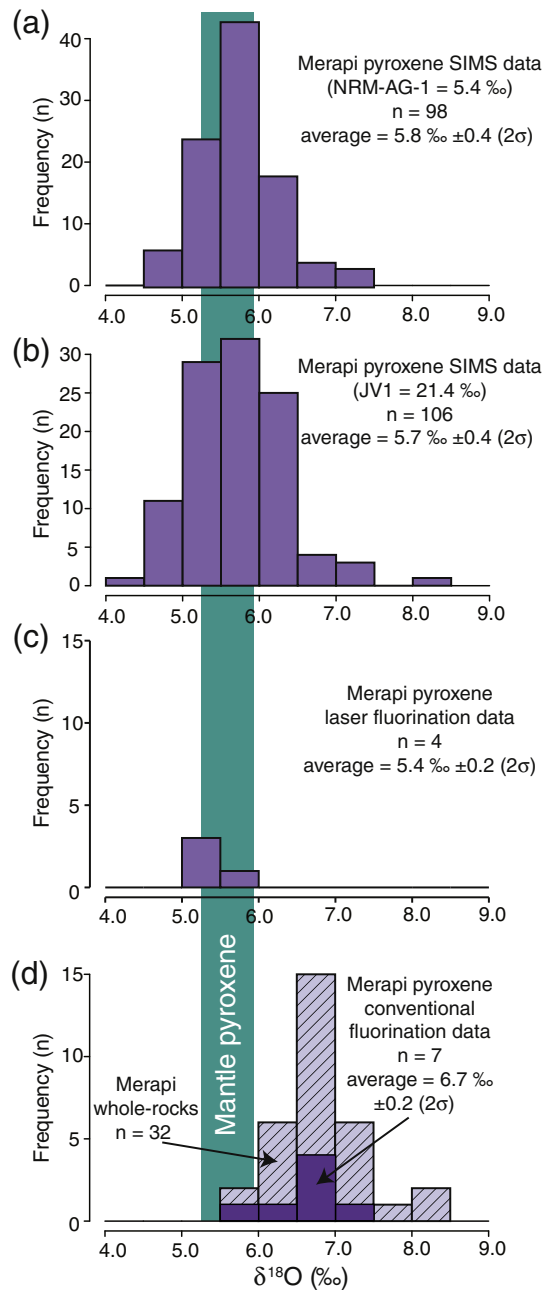


Fig. 5. (a, b) Frequency distribution plots of IMF-corrected $\delta^{18}\text{O}$ values of Merapi pyroxene obtained by SIMS and corrected to NRM-AG-1 in (a) and to JV1 in (b). (c) Frequency distribution plot of $\delta^{18}\text{O}$ values of Merapi pyroxene obtained by laser fluorination (from Troll et al., 2013), which agrees within error with the SIMS data in panels a) and b). (d) Frequency distribution plot of $\delta^{18}\text{O}$ values of Merapi whole-rocks and pyroxene mineral separates, obtained by conventional fluorination (from Gertisser and Keller, 2003; Troll et al., 2013). The range of $\delta^{18}\text{O}$ values of mantle clinopyroxene is shown for comparison (after Matthey et al., 1994). Note that Merapi whole-rocks and pyroxene separates are offset from mantle $\delta^{18}\text{O}$ values, probably due to incorporation of high $\delta^{18}\text{O}$ material such as foreign inclusions or groundmass with higher $\delta^{18}\text{O}$ values than the pyroxene (see text for further details).

As Merapi pyroxene are overall compositionally more Fe-rich than JV1 and hence more similar to NRM-AG-1, we re-processed our data using a normalised value for JV1 of 21.4‰, based on the results of our homogeneity tests. By adopting a matrix-adjusted value for JV1 of 21.4‰ instead of 20.3‰, we obtained a slightly higher range of $\delta^{18}\text{O}$ values for Merapi diopside, from 4.3 to 8.1‰ (Fig. 5b). These adjusted values not only show excellent overlap with the Merapi augite SIMS data, but they also display a better fit to the literature LF data (Fig. 5). We conclude that NRM-AG-1

is a more suitable standard to use for common andesitic pyroxene compositions similar to Merapi as it prevents the need to perform additional matrix-corrections, as illustrated in our test with JV1, which is notably Fe-poor. We also note here that JV1 is a metamorphic diopside sourced from marble in the Adirondack Mountains in the eastern USA (J. M. Eiler, pers. comm.) and is thus not fully appropriate for use during analysis of mafic arc magmas. Our comparative study thus underscores that composition-matched standardisation is of utmost importance in SIMS analysis and that JV1, for example, may not always be best suited for correcting the $\delta^{18}\text{O}$ values of calcic clinopyroxene compositions that have intermediate amounts of iron. Indeed, the difference in Mg-number (ratio of Fe to Mg in a mineral) between NRM-AG-1 and JV1 of nearly 20 units appears to have resulted in a bias effect of ca. 1‰ (cf. Fig. 2 and Fig. 3). We note here that a long-term goal in SIMS oxygen isotope analytical development is to understand which solid solutions in the pyroxene quadrilateral are most responsible for matrix effects. Although our data contribute towards this goal, a number of compositions would still need to be characterised and examined to cover the pyroxene solid solution series in full.

5.2.2. Estimate of primary $\delta^{18}\text{O}$ beneath Central Java

Merapi pyroxene are for the most part homogeneous with respect to their $\delta^{18}\text{O}$ values, however several crystals with resolvable isotopic heterogeneity were also identified (Fig. 6). This heterogeneity is for the most part unlikely to arise from sampling on cracks or included material just below the surface, because the samples were carefully screened before and after the SIMS sessions using SEM and optical microscopy and because secondary intensities did not fluctuate strongly during the analytical runs. The pyroxene $\delta^{18}\text{O}$ values obtained here average 5.8‰ (n = 204, 2SD = 1.2‰). It is important to note that the $\delta^{18}\text{O}$ values of pyroxene do not directly equate to mantle $\delta^{18}\text{O}$ values; the O-isotope

fractionation between pyroxene–magma at the time of crystallisation, fractionation between mantle and primary magma, and during fractional crystallisation, all need to be taken into account. For a basaltic andesite with $\text{SiO}_2 = 54$ wt.%, $D_{\text{pyroxene-magma}} = -0.6$ (using Table 2 of Bindeman et al., 2004). This means that the magma had a $\delta^{18}\text{O}$ value of 6.4‰. If it is assumed that the magma is entirely mantle-derived, and fractional crystallisation increased the $\delta^{18}\text{O}$ value by 0.3‰ (e.g. Bindeman et al., 2004) then the original “primary” magma would have had a $\delta^{18}\text{O}$ value of ~6.1‰. This is somewhat higher than the accepted value of MORB (5.7 ± 0.2 ‰, e.g. Eiler, 2001), and might indicate some crustal contamination. However, these are small differences and our pyroxene data (average = 5.8‰) are similar to the $\delta^{18}\text{O}$ values expected for pyroxene in mantle-derived magmas (cf. Harmon and Hoefs, 1995; Day et al., 2009; Fig. 5a and b) as well as to values obtained for pyroxene separates from other volcanic centres along the Sunda arc. For instance, $\delta^{18}\text{O}$ values of 5.3 to 5.6‰ and 5.5 to 5.9‰ were reported for Galunggung and Gede volcanoes in West Java, respectively (Harmon and Gerbe, 1992; Handley et al., 2010).

To test for the depth of pyroxene crystallisation, we employ the results of thermobarometric modelling described in Section 4.2. Assuming a crustal density of 2890 kg/m^3 (e.g. Nadeau et al., 2013), converted pyroxene crystallisation pressures yield a depth range of 9 to 21 km and indicate a main pyroxene storage interval at ca. 16 km depth, which translates to within the mid to deep crust under Java (Fig. 7). These results are in-line with previous thermobarometry studies at Merapi (Chadwick et al., 2013; Nadeau et al., 2013; Preece et al., 2014). The crust beneath Merapi includes Cretaceous to Tertiary limestone, marl, and volcanoclastic units extending to about 2 km depth (van Bemmelen, 1949), followed by sedimentary units ca. 8 to 11 km thickness (Smyth et al., 2005 and references therein), which is then underlain by a basement of uncertain, but probably crystalline character to

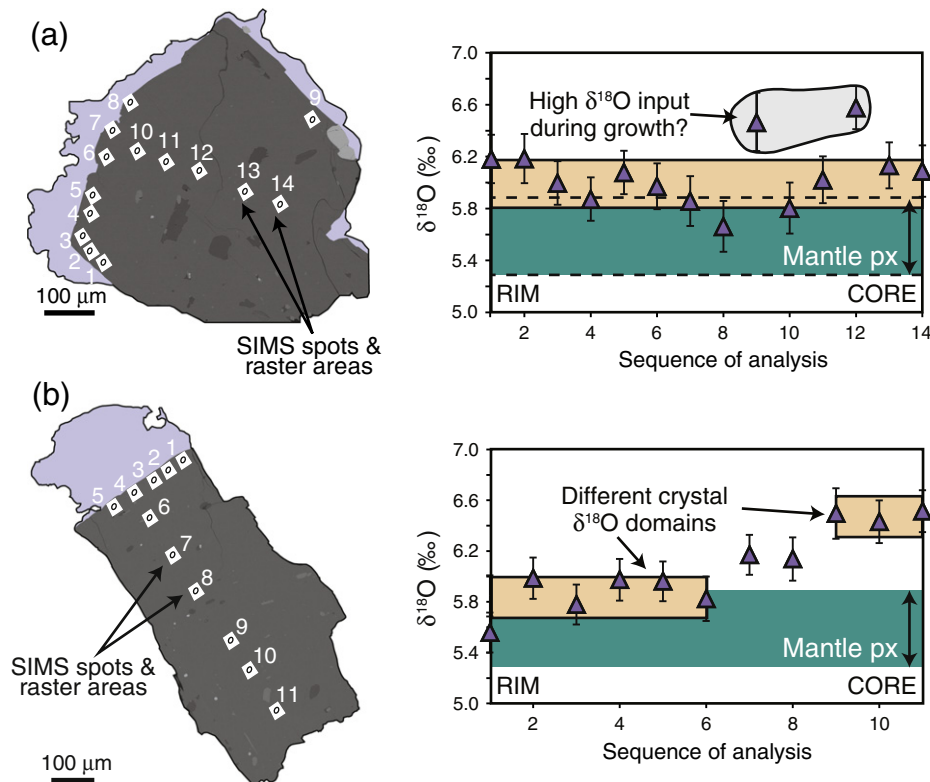


Fig. 6. Examples of $\delta^{18}\text{O}$ crystal isotope stratigraphy in representative Merapi augite. SIMS analysis spots are shown in the crystal sketches to the left, while variations in $\delta^{18}\text{O}$ values are illustrated in the plots to the right. Both crystals show resolvable isotopic heterogeneity, which is likely a common feature in igneous pyroxene and possibly reflects various processes during ascent and differentiation (e.g., magma mixing, assimilation, and recharge). Cream coloured boxes show the average $\delta^{18}\text{O}$ values for sub-groupings of the data and the height of the boxes corresponds to 2 standard deviations. These crystals formed at ca. 16 km depth, based on thermobarometry calculations discussed in Section 5.2.2 and both examples record minor and transient input of high $\delta^{18}\text{O}$ material during growth.

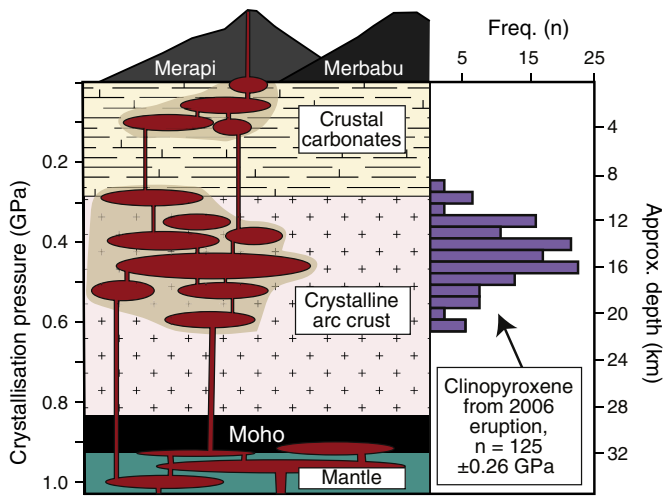


Fig. 7. Results of clinopyroxene composition barometry after Putirka (2008, Eq. 32b). The data show that the main pyroxene growth interval was located broadly at 16 km depth beneath Merapi, i.e. within the mid to deep crystalline arc crust. The schematic sketch of the magma plumbing system beneath Merapi (left) is drawn based on Chadwick et al. (2013), Preece et al. (2014), and this study. The Moho depth is taken from Wölbner and Rümpker (2016). While the analysed pyroxene have dominantly grown in the mid-crust, upper crustal storage and assimilation has also been identified in previous studies, especially in whole-rock and late grown plagioclase (e.g. Chadwick et al., 2013; Troll et al., 2013) and is likely reflected in some of the pyroxene $\delta^{18}\text{O}$ values reported here (e.g. Figs. 5 and 6).

about 25 to 30 km depth (Curry et al., 1977; Hamilton, 1979; Wölbner and Rümpker, 2016). Magma storage in the mid to deep crust is therefore consistent with an overall absence of significant sedimentary contamination recorded in the majority of Merapi pyroxene crystals investigated here.

A key benefit of the SIMS technique is that it enables the analyst to restrict analysis to uncompromised crystal areas, i.e., those that are devoid of melt and mineral inclusions, fractures, alteration zones, etc. This aspect of SIMS analysis is particularly useful for Merapi pyroxene that usually host an array of inclusions, such as those observed in 2006 Merapi eruptives (see Fig. 4). SIMS thus allows for a virtually pure pyroxene $\delta^{18}\text{O}$ value to be obtained, but care must be taken in the form of (i) pre- and post-analysis screening by optical light microscopy and SEM imaging and (ii) monitoring of secondary intensities during the analytical runs, to verify that the analysis spots did not sample unwanted material in the top 1 to 2 μm below the surface. In this respect, SIMS is an advantageous analytical method for analysing pure pyroxene $\delta^{18}\text{O}$ values with a degree of spatial control that cannot currently be replicated by any other method. This realisation is reflected in the frequency distribution plots of $\delta^{18}\text{O}$ values in Merapi pyroxene, which are markedly different for SIMS and LF versus bulk mineral and whole-rock data. While the SIMS and LF data show good overlap, the bulk mineral and whole-rock $\delta^{18}\text{O}$ data are offset to higher values, reaching up to 8.3‰ (Fig. 5d). Bearing in mind that a whole-rock analysis represents the sum of magmatic and post-magmatic processes recorded in the rock's history and that bulk mineral separates can be composed of up to 100's of crushed minerals, it appears that the primary $\delta^{18}\text{O}$ value is frequently obscured by bulk rock or bulk crystal approaches. Indeed, only a minor amount of the Merapi SIMS data extend to similarly high $\delta^{18}\text{O}$ values (Figs. 5 and 6). This comparison between data sets leads us to suggest that while most of the Merapi 2006 pyroxene in this study have $\delta^{18}\text{O}$ values consistent with crystallisation from a mantle-derived primary magma, some crystals yield higher and lower values which probably reflect an element of open system processes such as crustal assimilation or entrainment of xeno- or antecrysts that have undergone hydrothermal alteration from prolonged storage close to a heat source (see also Section 5.2.3 below).

5.2.3. Variability in $\delta^{18}\text{O}$ values in Merapi pyroxene

As noted above, the non-mantle-like $\delta^{18}\text{O}$ values observed in Merapi pyroxene can most likely be attributed to open-system processes because it is unlikely that these variations in pyroxene $\delta^{18}\text{O}$ values reflect individual and isotopically distinct mantle components. This would require mantle source changes on a similar timescale to pyroxene crystallisation, which is unfeasible (Turner et al., 1997; Davidson et al., 2005). Alternatively, differentiation processes such as crustal assimilation, fluid alteration, or magma mixing can occur on the timescales of crystal growth, and are therefore more likely to be preserved in the crystal record (cf. Chadwick et al., 2007; Deegan et al., 2010, 2011; Saunders et al., 2012). In this respect, we note that Merapi bulk pyroxene separates analysed by conventional fluorination have $\delta^{18}\text{O}$ values that range from 5.9 to 7.2‰, which is relatively high on average compared to the SIMS data (Fig. 5). The bulk pyroxene data might therefore reflect either (i) the presence of mineral or melt inclusions with high $\delta^{18}\text{O}$ values, (ii) fractures in the crystals along which low temperature meteoric water alteration to relatively high $\delta^{18}\text{O}$ values has occurred, (iii) incorporation of local carbonate or calc-silicate xenolithic material with high $\delta^{18}\text{O}$ values, or (iv) a combination of (i) to (iii). Whereas the effect of inclusions or fractures can be avoided by analysing inclusion and fracture-free domains by SIMS or choosing pristine crystals for LF, crustal assimilation can shift $\delta^{18}\text{O}$ values to either relatively high or low values, depending on the nature of the assimilate. Crustal components with high $\delta^{18}\text{O}$ values at Merapi include the carbonate basement and calc-silicate xenoliths ($\delta^{18}\text{O} \geq 10\text{‰}$; Troll et al., 2013). Conversely, high temperature hydrothermally altered crust is likely present at shallow levels beneath Merapi (Nadeau et al., 2013) and would be expected to have relatively low (sub-mantle) $\delta^{18}\text{O}$ values (e.g. Taylor and Sheppard, 1986; Donoghue et al., 2010), which if assimilated might cause a drop in the $\delta^{18}\text{O}$ values of the parent magma (cf. Bindeman et al., 2012). The tails in the pyroxene SIMS data towards high and low $\delta^{18}\text{O}$ values (relative to mantle) might thus reflect minor amounts of assimilation of isotopically diverse crustal material beneath Merapi. Since Merapi pyroxene crystallised dominantly in the mid to lower crust, e.g. in a major crystallisation region at ca. 16 km depth (Fig. 6; see also Chadwick et al., 2013; Preece et al., 2014), pyroxene mostly formed below the level of upper crustal carbonate-bearing lithologies, which is consistent with the dominantly mantle-like $\delta^{18}\text{O}$ values for pyroxene obtained here. Medium anorthite feldspar, on the other hand, is thought to crystallise at shallower depths beneath Merapi and is thus affected to a larger degree by crustal processes (Chadwick et al., 2007; Troll et al., 2013; Borisova et al., 2016).

Some Merapi pyroxene display a degree of isotopic diversity at the sub-crystal scale as demonstrated by crystal rims and cores that show differences in their $\delta^{18}\text{O}$ values outside the error limits of the analysis (1σ) (Fig. 6). Sub-crystal scale $\delta^{18}\text{O}$ variation has been frequently recognised in mineral phases such as olivine, quartz, and zircon (e.g. Valley and Graham, 1996; Jourdan et al., 2009; Eiler et al., 2011; Bindeman et al., 2012) and has been used as a window into processes such as crustal assimilation and hydrothermal fluid flow. A similar approach to resolving magmatic processes can now be employed using our proposed calcic clinopyroxene and orthopyroxene standards. These phases are almost ubiquitous components in intermediate arc volcanic rocks and in many cases crystallise to reasonably large sizes (i.e. several hundreds of micrometres across compared to e.g., zircon which is typically considerably smaller; see Fig. 4).

6. Conclusion

Accurate measurement of oxygen isotope ratios may be obtained for multiple pyroxene compositions by SIMS. Before SIMS analysis, the composition of pyroxene should be determined via, e.g. EPMA, in order to select the most appropriate, compositionally-matched standard for use during SIMS oxygen isotope analysis. We tested two new standard materials and subsequently the new standard NRM-AG-1

and the existing standard JV1 were successfully applied to well-documented samples from Merapi volcano, Indonesia. The new Merapi pyroxene SIMS data revealed a peak in $\delta^{18}\text{O}$ values at ca. 5.8‰, which suggests a primary magma composition of around 6.1‰ in Central Java. For this analytical session, we obtained a range in $\delta^{18}\text{O} \pm 0.5\%$ (2σ), which is sufficiently precise to allow detection of subtle inter-crystalline variations in $\delta^{18}\text{O}$ values. Moreover, employing the SIMS method to analyse the $\delta^{18}\text{O}$ values of pyroxene not only allows for high spatial resolution crystal transects to be analysed, but also increases confidence in obtaining pure crystal isotope values, since mineral-, melt-, and fluid-inclusions as well as alteration along fractures can be avoided. This is particularly pertinent for subduction zone volcanoes, where complex, multi-stage magmatic histories may be reflected in crystal zoning that is often accompanied by a relatively high density of inclusions. The new standards presented here now open up the possibility for high spatial resolution oxygen isotope crystal stratigraphy by SIMS of common pyroxene found in arc-type andesitic rocks.

Supplementary data to this article can be found online at <http://dx.doi.org/10.1016/j.chemgeo.2016.10.018>.

Acknowledgements

We are grateful for technical support from J. Majka and A. K. Barker at UU and L. Ilyinsky and K. Lindén at NRM Stockholm. We also thank research assistant L. Barke for help drafting the pyroxene composition diagrams and T. E. Waight, F. Weis, J. M. Eiler, and P. J. le Roux for helpful discussions. T. Tenner and an anonymous reviewer are acknowledged for thorough reviews that helped improve the manuscript, and D. R. Hilton is thanked for editorial handling. This work was supported by the Swedish Research Council (VR, grant number 621-2013-5628), the Swedish Foundation for International Cooperation in Research and Higher Education (STINT, grant number SA2015-6212), and the National Research Foundation (NRF) of South Africa. The NordSIM facility is supported by the research funding agencies of Denmark, Iceland, Norway and Sweden, the Geological Survey of Finland, and the Swedish Museum of Natural History. This is NordSIM publication #479.

References

- Baertschi, P., 1976. Absolute ^{18}O content of standard mean ocean water. *Earth Planet. Sci. Lett.* 31, 341–344.
- Barker, A.K., Troll, V.R., Carracedo, J.C., Nicholls, P.A., 2015. The magma plumbing system for the 1971 Teneguía eruption, La Palma, Canary Islands. *Contrib. Mineral. Petrol.* 170, 1–21.
- Bindeman, I.N., Valley, J.W., 2000. Formation of low- $\delta^{18}\text{O}$ rhyolites after caldera collapse at Yellowstone, Wyoming, USA. *Geology* 28, 719–722.
- Bindeman, I.N., Ponomareva, V.V., Bailey, J.C., Valley, J.W., 2004. Volcanic arc of Kamchatka: a province with high- ^{18}O magma sources and large-scale $^{18}\text{O}/^{16}\text{O}$ depletion of the upper crust. *Geochim. Cosmochim. Acta* 68, 841–865.
- Bindeman, I.N., Gurenko, A., Carley, T., Miller, C., Martin, E., Sigmarsson, O., 2012. Silicic magma petrogenesis in Iceland by remelting of hydrothermally altered crust based on oxygen isotope diversity and disequilibria between zircon and magma with implications for MORB. *Terra Nova* 24, 227–232.
- Borisova, A.Y., Martel, C., Gouy, S., Pratomo, I., Sumatri, S., Toutain, J.-P., Bindeman, I.N., de Parseval, P., Metaxian, J.-P., Surono, 2013. Highly explosive 2010 Merapi eruption: evidence for shallow-level crustal assimilation and hybrid fluid. *J. Volcanol. Geotherm. Res.* 261, 193–208.
- Borisova, A.Y., Gurenko, A.A., Martel, C., Kouzmanov, K., Cathala, A., Bohrsen, W.A., Pratomo, I., Sumarti, S., 2016. Oxygen isotope heterogeneity of arc magma recorded in plagioclase from the 2010 Merapi eruption (Central Java, Indonesia). *Geochim. Cosmochim. Acta* 190, 13–34.
- Chadwick, J.P., Troll, V.R., Ginibre, C., Morgan, D., Gertisser, R., Waight, T.E., Davidson, J.P., 2007. Carbonate assimilation at Merapi volcano, Java, Indonesia: insights from crystal isotope stratigraphy. *J. Petrol.* 48, 1793–1812.
- Chadwick, J.P., Troll, V.R., Waight, T.E., van der Zwan, F.M., Schwarzkopf, L.M., 2013. Petrology and geochemistry of igneous inclusions in recent Merapi deposits: a window into the sub-volcanic plumbing system. *Contrib. Mineral. Petrol.* 166, 43–63.
- Chiba, H., Chacko, T., Clayton, R.N., Goldsmith, J.R., 1989. Oxygen isotope fractionations involving diopside, forsterite, magnetite, and calcite: application to geothermometry. *Geochim. Cosmochim. Acta* 53, 2985–2995.
- Costa, F., Andreastuti, S., Bouvet de Maisonneuve, C., Pallister, J.S., 2013. Petrological insights into the storage conditions, and magmatic processes that yielded the centennial 2010 Merapi explosive eruption. *J. Volcanol. Geotherm. Res.* 261, 209–235.
- Curry, J.R., Shor, G.G., Raitt, R.W., Henry, M., 1977. Seismic refraction and reflection studies of crustal structure of the eastern Sunda and western Banda arcs. *J. Geophys. Res.* 82, 2479–2489.
- Dahren, B., Troll, V.R., Andersson, U.B., Chadwick, J.P., Gardner, M.F., Jaxybulatov, K., Koulakov, I., 2012. Magma plumbing beneath Anak Krakatau volcano, Indonesia: evidence for multiple magma storage regions. *Contrib. Mineral. Petrol.* 163, 631–651.
- Davidson, J.P., Hora, J.M., Garrison, J.M., Dungan, M.A., 2005. Crustal forensics in arc magmas. *J. Volcanol. Geotherm. Res.* 140, 157–170.
- Day, J.M.D., Pearson, D.G., Macpherson, C.G., Lowry, D., Carracedo, J.C., 2009. Pyroxenite-rich mantle formed by recycled oceanic lithosphere: oxygen-osmium isotope evidence from Canary Island lavas. *Geology* 37, 555–558.
- Deegan, F.M., Troll, V.R., Freda, C., Misiti, V., Chadwick, J.P., McLeod, C., Davison, J.P., 2010. Magma-carbonate interaction processes and associated CO_2 release at Merapi volcano, Indonesia: insights from experimental petrology. *J. Petrol.* 51, 1027–1051.
- Deegan, F.M., Troll, V.R., Freda, C., Misiti, V., Chadwick, J.P., 2011. Fast and furious: crustal CO_2 release at Merapi volcano, Indonesia. *Geol. Today* 27, 63–64.
- Donoghue, E., Troll, V.R., Harris, C., 2010. Fluid-rock interaction in the Miocene, post-caldera, Tejeda intrusive complex, Gran Canaria (Canary Islands): insights from mineralogy, and O and H-isotope geochemistry. *J. Petrol.* 51, 2149–2176.
- Eiler, J.M., 2001. Oxygen isotope variations of basaltic lavas and upper mantle rocks. *Rev. Mineral.* 43, 319–364.
- Eiler, J.M., Graham, C., Valley, J.W., 1997. SIMS analysis of oxygen isotopes: matrix effects in complex minerals and glasses. *Chem. Geol.* 138, 221–244.
- Eiler, J.M., Stolper, E.M., McCanta, M., 2011. Intra- and intercrystalline oxygen isotope variations in minerals from basalts and peridotites. *J. Petrol.* 52, 1393–1413.
- Ferry, J.M., Kitajima, K., Strickland, A., Valley, J.W., 2014. Ion microprobe survey of the grain-scale oxygen isotope geochemistry of minerals in metamorphic rocks. *Geochim. Cosmochim. Acta* 144, 403–433.
- Gertisser, R., Keller, J., 2003. Trace element and Sr, Nd, Pb and O isotope variations in medium-K and high-K volcanic rocks from Merapi volcano, Central Java, Indonesia: evidence for the involvement of subducted sediments in Sunda arc magma genesis. *J. Petrol.* 44, 457–489.
- Gurenko, A.A., Chaussidon, M., 2002. Oxygen isotope variations in primitive tholeiites of Iceland: evidence from a SIMS study of glass inclusions, olivine phenocrysts and pillow rim glasses. *Earth Planet. Sci. Lett.* 205, 63–79.
- Hamilton, W., 1979. Tectonics of the Indonesian Region. US Geological Survey, Professional Papers. 1078, pp. 1–345.
- Handley, H.K., Macpherson, C.G., Davidson, J.P., 2010. Geochemical and Sr-O isotopic constraints on magmatic differentiation at Gede volcanic complex, West Java, Indonesia. *Contrib. Mineral. Petrol.* 159, 885–908.
- Harmon, R.S., Gerbe, M.-C., 1992. The 1982–83 eruption at Galunggung volcano, Java (Indonesia): oxygen isotope geochemistry of a chemically zoned magma chamber. *J. Petrol.* 33, 585–609.
- Harmon, R.S., Hoefs, J., 1995. Oxygen isotope heterogeneity of the mantle deduced from global ^{18}O systematics of basalts from difference tectonic settings. *Contrib. Mineral. Petrol.* 120, 95–114.
- Harris, C., Vogeli, J., 2010. Oxygen isotope composition of garnet in the Peninsula Granite, Cape Granite Suite, South Africa: constraints on melting and emplacement mechanisms. *S. Afr. J. Geol.* 113, 401–412.
- Hartley, M.E., Thordarson, T., Taylor, C., Fitton, J.G., EIMF, 2012. Evaluation of the effects of composition on instrumental mass fractionation during SIMS oxygen isotope analyses of glasses. *Chem. Geol.* 334, 312.
- Hoefs, J., 1973. *Stable Isotope Geochemistry*. Springer-Verlag, Berlin (145 pp).
- Huberty, J.M., Kita, N.T., Kozdon, R., Heck, P.R., Fournelle, J.H., Spicuzza, M.J., Xu, H., Valley, J.W., 2010. Crystal orientation effects in $\delta^{18}\text{O}$ for magnetite and hematite by SIMS. *Chem. Geol.* 276, 269–283.
- Hyodo, A., Kozdon, R., Pollington, A.D., Valley, J.W., 2014. Evolution of quartz cementation and burial history of the Eau Claire formation based on in situ oxygen isotope analysis of quartz overgrowths. *Chem. Geol.* 384, 168–180.
- Jeffery, A.J., Gertisser, R., Troll, V.R., Jolis, E.M., Dahren, B., Harris, C., Tindle, A.G., Preece, K., O'Driscoll, B., Humaida, H., Chadwick, J.P., 2013. The pre-eruptive magma plumbing system of the 2007–2008 dome-forming eruption of Kelut volcano, East Java, Indonesia. *Contrib. Mineral. Petrol.* 166, 275–308.
- Jochum, K.P., Stoll, B., Herwig, K., Willbold, M., Hofmann, A.W., Amini, M., Aarburg, S., Abouchami, W., Hellebrand, E., Mocek, B., Raczek, I., Stracke, A., Alard, O., Bouman, C., Becker, S., Dücking, M., Brätz, H., Klemm, R., de Bruin, D., Canil, D., Cornell, D., de Hoog, C.-J., Dalpé, C., Danyushevsky, L., Eisenhauer, A., Gao, Y., Snow, J.E., Groschopf, N., Günther, D., Latkoczy, C., Guillong, M., Hauri, E.H., Höfer, H.E., Lahaye, Y., Horz, K., Jacob, D.E., Kasemann, S.A., Kent, A.J.R., Ludwig, T., Zack, T., Mason, P.R.D., Meixner, A., Rosner, M., Misawa, K., Nash, B.P., Pfänder, J., Premo, W.R., Sun, W.D., Tiepolo, M., Vannucci, R., Vennemann, T., Wayne, D., Woodhead, J.D., 2006. MPI-DING reference glasses for in situ microanalysis: new reference values for element concentrations and isotope ratios. *Geochim. Geophys. Geosyst.* 7, Q02008.
- Jourdan, A.-L., Vennemann, T.W., Mullis, J., Ramseyer, K., 2009. Oxygen isotope sector zoning in natural hydrothermal quartz. *Mineral. Mag.* 73, 615–632.
- Kita, N.T., Ikeda, Y., Togashi, S., Liu, Y., Morishita, Y., Weisberg, M.K., 2004. Origin of urelites inferred from a SIMS oxygen isotopic and trace element study of clasts in the Dar al Gani 319 polymict urelite. *Geochim. Cosmochim. Acta* 68, 4213–4235.
- Kita, N.T., Ushikubo, T., Fu, B., Valley, J.W., 2009. High precision SIMS oxygen isotope analysis and the effect of sample topography. *Chem. Geol.* 264, 43–57.
- Matthey, D., Lowry, D., Macpherson, C., 1994. Oxygen isotope composition of mantle peridotite. *Earth Planet. Sci. Lett.* 128, 231–241.
- Mora, C.I., Riciputi, L.R., Cole, D.R., Walker, K.D., 2009. High-temperature hydrothermal alteration of the Boehls Butte anorthosite: origin of a bimodal plagioclase assemblage. *Contrib. Mineral. Petrol.* 157, 781–795.

- Nadeau, O., Williams-Jones, A.E., Stix, J., 2013. Magmatic-hydrothermal evolution and devolatilisation beneath Merapi volcano, Indonesia. *J. Volcanol. Geotherm. Res.* 261, 50–68.
- Nemchin, A.A., Pidgeon, R.T., Whitehouse, M.J., 2006a. Re-evaluation of the origin and evolution of >4.2 Ga zircons from the Jack Hills metasedimentary rocks. *Earth Planet. Sci. Lett.* 244, 218–233.
- Nemchin, A.A., Whitehouse, M.J., Pidgeon, R.T., Meyer, C., 2006b. Oxygen isotopic signature of 4.4–3.9 Ga zircons as a monitor of differentiation processes on the moon. *Geochim. Cosmochim. Acta* 70, 1864–1872.
- Nemchin, A.A., Humayun, M., Whitehouse, M.J., Hewins, R.H., Lorand, J.-P., Kennedy, A., Grange, M., Zanda, B., Fieni, C., Deldicque, D., 2014. Record of the ancient martian hydrosphere and atmosphere preserved in zircon from a martian meteorite. *Nat. Geosci.* 7, 638–642.
- Nimis, P., 1995. A clinopyroxene geobarometer for basaltic systems based on crystal-structure modelling. *Contrib. Mineral. Petrol.* 121, 115–125.
- Page, F.Z., Ushikubo, T., Kita, N.T., Riciputi, L.R., Valley, J.W., 2007. High-precision oxygen isotope analysis of pictogram samples reveals 2 μm gradients and slow diffusion in zircon. *Am. Mineral.* 92, 1772–1775.
- Page, F.Z., Kita, N., Valley, J.W., 2010. Ion microprobe analysis of oxygen isotopes in garnets of complex chemistry. *Chem. Geol.* 270, 9–19.
- Preece, K., Gertisser, R., Barclay, J., Berlo, K., Herd, R.A., Facility, E.I.M., 2014. Pre- and syn-eruptive degassing and crystallisation processes of the 2010 and 2006 eruptions of Merapi volcano, Indonesia. *Contrib. Mineral. Petrol.* 168, 1061.
- Prescher, C., McCammon, C., Dubrovinsky, L., 2012. MossA: a program for analyzing energy-domain Mössbauer spectra from conventional and synchrotron sources. *J. Appl. Crystallogr.* 45, 329–331.
- Putirka, K.D., 2008. Thermometers and barometers for volcanic systems. *Rev. Mineral. Geochem.* 69, 61–120.
- Riciputi, L.R., Paterson, B.A., Ripperdan, R.L., 1998. Measurement of light stable isotope ratios by SIMS: matrix effects for oxygen, carbon, and sulfur isotopes in minerals. *Int. J. Mass Spectrom.* 178, 81–112.
- Saunders, K., Blundy, J., Dohmen, R., Cashman, K., 2012. Linking petrology and seismology at an active volcano. *Science* 336, 1023–1027.
- Sláma, J., Košler, J., Condon, D.J., Crowley, J.L., Gerdes, A., Hanchan, J.M., Horstwood, M.S.A., Morris, G.A., Nasdala, L., Norberg, N., Schaltegger, U., Schoene, B., Tubrett, M.N., Whitehouse, M.J., 2008. Plešovice zircon – a new natural reference material for U–Pb and Hf isotopic microanalysis. *Chem. Geol.* 249, 1–35.
- Śliwiński, M.G., Kitajima, K., Kozdon, R., Spicuzza, M.J., Fournelle, J.H., Debby, A., Valley, J.W., 2016. Secondary ion mass spectrometry bias on isotope ratios in dolomite-ankerite, part 1: $\delta^{18}\text{O}$ matrix effects. *Geostand. Geoanal. Res.* 40, 157–172.
- Smyth, H.R., Hall, R., Hamilton, J., Kinny, P., 2005. East Java: Cenozoic basins, volcanoes and ancient basement. Proceedings, Indonesian Petroleum Association, Thirtieth Annual Convention & Exhibition.
- Taylor, H.P., Sheppard, S.M.F., 1986. Igneous rocks: I. Processes of isotopic fractionation and isotope systematics. In: Valley, J.W., Taylor, H.P., O'Neill, J.R. (Eds.), *Stable Isotopes in High Temperature Geological Processes. Reviews in Mineralogy* 16, pp. 227–269.
- Tenner, T.J., Ushikubo, T., Kurahashi, E., Kita, N.T., Nagahara, H., 2013. Oxygen isotope systematics of chondrule phenocrysts from the CO3.0 chondrite Yamato 81020: evidence for two distinct oxygen isotope reservoirs. *Geochim. Cosmochim. Acta* 102, 226–245.
- Troll, V.R., Deegan, F.M., Jolis, E.M., Harris, C., Chadwick, J.P., Gertisser, R., Schwarzkopf, L.M., Borisova, A.Y., Bindeman, I.N., Sumarti, S., Preece, K., 2013. Magmatic differentiation processes at Merapi volcano: inclusion petrology and oxygen isotopes. *J. Volcanol. Geotherm. Res.* 261, 38–49.
- Troll, V.R., Deegan, F.M., Jolis, E.M., Budd, D.A., Dahren, B., Schwarzkopf, L., 2015. Ancient oral tradition describes volcano-earthquake interaction at Merapi volcano, Indonesia. *Geografiska Annaler: Series A, Physical Geography* 97, 137–166.
- Turner, S., Hawkesworth, C., Rogers, N., Bartlett, J., Worthington, T., Hergt, J., Pearce, J., Smith, I., 1997. ^{238}U – ^{230}Th disequilibria, magma petrogenesis, and flux rates beneath the depleted Tonga-Kermadec island arc. *Geochim. Cosmochim. Acta* 61, 4855–4884.
- Valley, J.W., Graham, C.M., 1996. Ion microprobe analysis of oxygen isotope ratios in quartz from Skye granite: healed micro-cracks, fluid flow, and hydrothermal exchange. *Contrib. Mineral. Petrol.* 124, 225–234.
- Valley, J.W., Kita, N.T., 2009. In situ oxygen isotope geochemistry by ion microprobe. In: Fayek, M. (Ed.), *Secondary Ion Mass Spectrometry in the Earth Sciences* 41. Mineralogical Association of Canada Short Course, pp. 19–63.
- Valley, J.W., Kitchen, M., Kohn, M.J., Niendorf, C.R., Spicuzza, M.J., 1995. UWG-2, a garnet standard for oxygen isotope ratios: strategies for high precision and accuracy with laser heating. *Geochim. Cosmochim. Acta* 59, 5223–5231.
- Valley, J.W., Reinhard, D.A., Cavosie, A.J., Ushikubo, T., Lawrence, D.F., Larson, D.J., Kelly, T.F., Snoeyenbos, D.R., Strickland, A., 2015. Nano- and micro-geochronology in Hadean and Archean zircons by atom-probe tomography and SIMS: new tools for old minerals. *Am. Mineral.* 100 (in press).
- van Bemmelen, R.W., 1949. *The Geology of Indonesia, 1A, General Geology*. Government Printing Office, The Hague.
- van der Zwan, F.M., Chadwick, J.P., Troll, V.R., 2013. Textural history of recent basaltic-andesites and plutonic inclusions from Merapi volcano. *Contrib. Mineral. Petrol.* 166, 43–63.
- Weis, F.A., Stalder, R., Skogby, H., 2016. Experimental hydration of natural volcanic clinopyroxene phenocrysts under high pressure (0.5–3 kbar). *Am. Mineral.* 101, 2233–2247.
- Whitehouse, M.J., Nemchin, A.A., 2009. High precision, high accuracy measurement of oxygen isotopes in a large lunar zircon by SIMS. *Chem. Geol.* 261, 32–42.
- Wiedenbeck, M., Hanchan, J.M., Peck, W.H., Sylvester, P., Valley, J., Whitehouse, M.J., Kronz, A., Morishita, Y., Nasdala, L., Fiebig, J., Franchi, I., Girard, J.-P., Greenwood, R.C., Hinton, R., Kita, N., Mason, P.R.D., Norman, M., Ogasawara, M., Piccoli, P.M., Rhede, D., Satoh, H., Schulz-Dobrick, B., Skår, O., Spicuzza, M.J., Terada, K., Tindle, A., Togashi, S., Vennemann, T., Xie, Q., Zheng, Y.-F., 2004. Further characterisation of the 91500 zircon crystal. *Geostand. Geoanal. Res.* 28, 9–39.
- Winpenny, B., MacLennan, J., 2014. Short length scale oxygen isotope heterogeneity in the Icelandic mantle: evidence from plagioclase compositional zones. *J. Petrol.* 55, 2537–2566.
- Wölbern, I., Rumpker, G., 2016. Crustal thickness beneath Central and East Java (Indonesia) inferred from P receiver functions. *J. Asian Earth Sci.* 115, 69–79.